ISSN 1063-7745, Crystallography Reports, 2021, Vol. 66, No. 5, pp. 777–785. © The Author(s), 2021. This article is an open access publication, corrected publication 2021.
Russian Text © The Author(s), 2021, published in Kristallografiya, 2021, Vol. 66, No. 5, pp. 750–758.

STRUCTURE OF MACROMOLECULAR COMPOUNDS

Crystallization in Microgravity and the Atomic-Resolution Structure of Uridine Phosphorylase from *Vibrio cholerae*

P. A. Eistrikh-Heller[a], S. V. Rubinsky[a], V. R. Samygina[a,b], A. G. Gabdulkhakov[a], M. V. Kovalchuk[a,b], A. S. Mironov[c], and A. A. Lashkov[a,*]

[a] *Shubnikov Institute of Crystallography of Federal Scientific Research Centre "Crystallography and Photonics," Russian Academy of Sciences, Moscow, 119333 Russia*

[b] *National Research Center "Kurchatov Institute," Moscow, 117545 Russia*

[c] *Engelhardt Institute of Molecular Biology, Russian Academy of Sciences, Moscow, 119991 Russia*

**e-mail: alashkov83@gmail.com*

Received September 8, 2020; revised September 22, 2020; accepted September 28, 2020

Abstract—Uridine phosphorylases are known as key targets for the development of new anticancer and antiparasitic agents. Crystals of uridine phosphorylase from the pathogenic bacterium *Vibrio cholerae* were grown in microgravity by the capillary counter-diffusion method on board of the International Space Station. The three-dimensional structure of this enzyme was determined at atomic (1.04 Å) resolution (RCSB PDB ID: 6Z9Z). Alternative conformations of long fragments (β-strands and adjacent loops) of the protein molecule were found for the first time in the three-dimensional structure of uridine phosphorylase in the absence of specific bound ligands. Apparently, these alternative conformations are related to the enzyme function. Conformational analysis with Markov state models demonstrated that conformational rearrangements can occur in the ligand-free state of the enzyme.

DOI: 10.1134/S1063774521050059

INTRODUCTION

In human cells, the demand for pyrimidine nitrogenous bases, in particular thymine and uridine, increases during the cancer disease development. Nitrogenous bases are produced by the reversible phosphorolytic cleavage of pyrimidine nucleosides. This reaction is catalyzed by uridine phosphorylase (UPh). The expression of this protein is upregulated in cancer cells [1–3]. Therefore, some anticancer drugs are targeted to the regulation of metabolism of nitrogenous bases and their derivatives. In particular, UPh inhibitors can be used as such drugs. They regulate the metabolism of such nitrogenous bases as uridine and thymidine, the resynthesis of which involves UPh.

Currently, great attention is given to the evaluation of the enzyme specificity of UPh and the development of reversible competitive inhibitors, the decrease in the concentration of which leads to the restoration of UPh activity. The structures of the protein from different organisms and its complexes with various ligands were determined and characterized at a resolution of up to 1.2 Å [4–13].

The development of UPh inhibitors as new drugs requires an understanding of the mechanisms of protein action. This issue can be addressed by determining the crystal structures of the protein and its complexes with high accuracy by means of X-ray crystallography. According to our experience, an analysis of the structures determined at atomic and subatomic resolution makes it possible not only to reveal the structural features of the protein and its complexes but also to elucidate the mechanism of action of the enzyme as a biological machine relying on experimental data by analyzing alternative conformations, anisotropic displacement parameters, and active-site protonation states [6, 10, 11].

Crystallization in microgravity is a promising tool for growing crystals of macromolecules. As it was demonstrated in [14–16], the crystals grown in microgravity have a more ordered internal structure, reduced twinning, and higher scattering ability compared to the Earth-grown crystals.

Here, we report the X-ray diffraction study of the crystal structure of uridine phosphorylase from *Vibrio cholerae* (*Vch*UPh) using crystals grown in microgravity on board of the International Space Station (ISS). Alternative conformations of long secondary-structure elements (β-stands and loops) of the protein tertiary structure in the absence of specific bound ligands were analyzed. Previously, alternative conformations in the atomic-resolution UPh structures were observed only in complexes of UPh with functionally important ligands bound at partial occupancy [6, 10, 11].

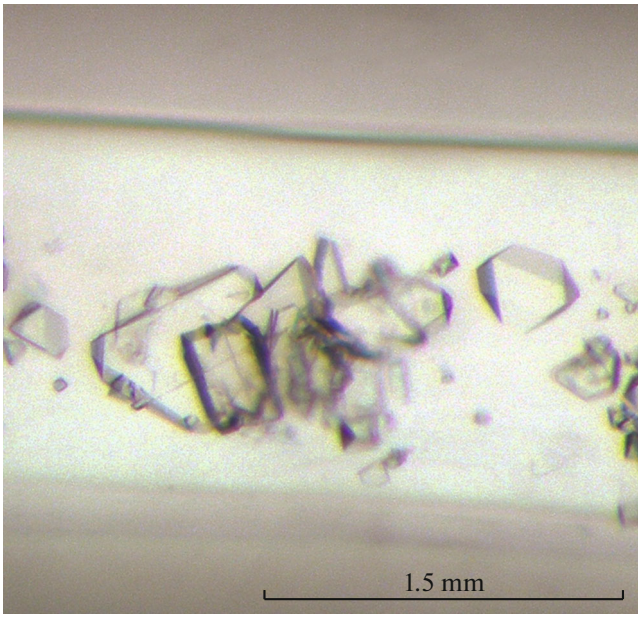

Fig. 1. Crystals of uridine phosphorylase from *V. cholerae* grown in microgravity.

MATERIALS AND METHODS

Isolation and Purification of VchUPh

The enzyme *Vch*UPh was purified by two-step ion-exchange chromatography on butyl-Sepharose and *Q*-Sepharose (Amersham Pharmacia Biotech) in the first and second steps, respectively. According to SDS gel electrophoresis, the homogeneity of *Vch*UPh was 96%. The procedures for the harvesting of the biomass of the producer and for the isolation and purification of *Vch*UPh were described in [8].

Crystallization

The protein crystallization by the vapor-diffusion technique was described in [8, 10]. The protein concentration was 15 mg/mL in 0.1 M Tris-HCl buffer. The reservoir solution was composed of 0.2 M $MgCl_2 \cdot 6H_2O$, 15 wt % polyethylene glycol (PEG) 4000, and 0.1 M Tris-HCl, pH 8.5.

The crystallization conditions found by the vapor-diffusion technique were then adapted to apply the capillary counter-diffusion technique in microgravity crystallization experiments. The known crystallization conditions served as the starting point. Then the magnesium chloride concentration was varied from 0.1 to 0.4 M, and the PEG 4000 concentrations was varied from 15 to 25% with a step of 2%. The crystallization was performed by the capillary counter-diffusion method [17] on board of the ISS. A control crystallization experiment using the same crystallization conditions was repeated in parallel in a laboratory on Earth. In the control experiment, crystals suitable for X-ray diffraction appeared within two weeks. The X-ray diffraction data set was collected from the crystals (Fig. 1) grown at 293 K in microgravity using the following conditions: 0.1 M Tris-HCl, pH 8.5, supplemented with 0.3 M $MgCl_2 \cdot 6H_2O$ and 19 wt % PEG 4000.

X-ray Diffraction Data Collection and Processing

The X-ray diffraction data set was collected from a crystal of *Vch*UPh on the BL41XU beamline at the SPring-8 synchrotron facility (Hyogo, Japan) at 100 K. The cryoprotectant solution was composed of the components of the reservoir solution with the addition of 20% glycerol The experimental intensities of reflections were processed with the XDS program package [18]. The intensities were scaled and the structure factor magnitudes were calculated using the SCALA program [19]. The X-ray diffraction data collection and processing statistics are given in Table 1.

Structure Solution and Refinement

The structure was solved by the molecular replacement method with the Molrep program [20]. The *Vch*UPh structure (PDB ID: 6EYP) was used as the starting model. The structure was refined with the phenix.refine program [21] combined with the manual rebuilding of the model using the Coot interactive graphics program [22]. The following non-specific ligands bound to the protein were found in the structure: glycerol, 1,2-ethanediol, diethylene glycol, magnesium ions, and sodium ions. The atomic displacement parameters were refined anisotropically. In the final cycles of the refinement, hydrogen atoms were included in the structural model. The validation of the structure refinement was performed with the ProCheck [23] and MolProbity [24] programs and using the PDB Validation Server (http://validate.rcsb.org). The structure refinement statistics are given in Table 1. The structure was deposited in the Research Collaboratory for Structural Bioinformatics Protein Data Bank (RCSB-PDB; PDB ID: 6Z9Z).

Classical Molecular Dynamics Simulations

To found the most probable conformations of the main-chain regions involved in the enzyme active site and evaluate the binding stability of glycerol to the enzyme, we performed molecular dynamics (MD) simulations of this complex with the GROMACS software package (version 2018.8) [25], using the CHARMM all-atom force field [26] of version C36m [27]. The ligand models were parameterized with CGenFF server [28]. Water molecules were described by the three-site TIP3P model. Magnesium and chloride ions were added to the system to provide a concentration corresponding to 0.3 M $MgCl_2$. Long-range electrostatic interactions were calculated by the particle-mesh method with a cubic interpolation

function. Van-der-Waals interactions were approximated by the "force-switch" function in a range from 10 to 12 Å. The pressure in the system was controlled with the Parrinello–Rahman pressure coupling algorithm [29] at 1 bar. The temperature of the MD system was kept constant with the temperature coupling algorithm (V-rescale [30]) at 293 K (corresponds to the temperature at which crystallization process was carried out). The MD trajectory was set to 100 ns. Newton's equations of motion were integrated with a step of 2 fs using the leap-frog algorithm. A total of four trajectories were obtained for the dimer CD, including two trajectories of the A conformer in the presence and in the absence of a glycerol molecule and two trajectories of the B conformer also in the presence and in the absence of glycerol.

Determination of the Relative Binding Affinity of Glycerol to the Active Site of VchUPh by the Linear Interaction Energy Method

The relative binding affinity of glycerol was calculated by the linear interaction energy (LIE) method [31] using the gmx_lie program implemented in the GROMACS software package. The molecular dynamics trajectories for protein–ligand interactions were again calculated by the reaction-field method at a cutoff of 15 Å to evaluate the potential energy of Coulomb interactions between the ligand and the environment. Then the MD trajectories were calculated throughout the time frame, during which glycerol does not leave the active site of UPh (4.2 and 1 ns for the alternative A and B conformations, respectively).

Molecular Dynamics Simulations Coupled with Markov State Models

The method of Markov state models [32] was used with the PyEmma software package [33] for interpretation of the molecular modelling results. To reduce the dimensionality of the data to a set of variables that determine the conformational properties of the polypeptide chain, we used the sines and cosines of the main-chain dihedral angles for the chain D of *Vch*UPh for the residue regions 90–107, 144–153, and 215–226. In order to further reduce the dimensionality of the conformational space, we applied the time-lagged independent component analysis (TICA) [34]. In this step, the correlation functions were calculated so as to obtain the maximum autocorrelation coefficients and reduce the correlation between different variables to zero, which allowed us to additionally reduce the dimensionality of the data by the conversion to the so-called independent coordinates. The lag times were selected based on the times typical of similar conformational changes in other proteins [35]. Hence, the further adjustment was performed after the analysis of the supposed time ranges of transitions between the

Table 1. X-ray diffraction data-collection and processing and the structure solution and refinement statistics

X-ray diffraction data statistics	
Wavelength, Å	0.7
Detector	EIGER 16M
Crystal-to-detector distance, mm	190
Oscillation angle, deg	0.1
Space group	$P2_1$
a, b, c, Å	93.186, 97.061, 93.227
$\alpha = \gamma$, β, deg	90.00; 119.965
Resolution, Å	46.59–1.04 (1.08–1.04)*
Total number of reflections	2680710 (268036)*
Number of unique reflections	682103 (67467)*
Completeness of data, %	99.15 (98.57)*
Redundancy	3.9 (4.0)*
Average value $\langle I/\sigma(I)\rangle$	12.64 (1.56)*
Overall Wilson temperature factor, Å^2	10.16
R_{merge}, %	5.56 (82.41)*
R_{meas}, %	6.41 (94.98)*
R_{pim}, %	3.16 (46.72)*
$CC_{1/2}$, %	99.8 (63.6)*
Structure refinement	
Cut-off Sigma, min($\sigma(\|F\|)/\|F\|$)	2.0
Number of reflections in the working set	679672 (67460)*
Number of reflections in the test set	33812 (3492)*
R_{work}, %	12.56 (23.27)*
R_{free}, %	14.20 (24.36)*
Cruickshank DPI, Å	0.029
Number of refined non-hydrogen atoms	
Protein	12501
Ligands	105
Water	1688
Rms deviation from ideal geometry	
Bond lengths, Å	0.007
Bond angles, deg	0.96
Average B factor for all atoms, Å^2	16.27
Macromolecule	14.39
Ligands	32.47
Water	29.23
Ramachandran plot	
Number of residues in the most favored regions, %	98.79
Number of residues in additionally allowed regions, %	0.81
Number of outliers, %	0.4
Rotamer outliers, %	0.73
PDB ID	6Z9Z

$CC_{1/2}$ is the Pearson's correlation coefficient between the measured intensities of two randomly assigned half-subsets of reflections in the overall data set.

* The data for the last high-resolution shell are given in parentheses.

major states of the Markov model [36]. For the regions of the molecule under consideration (residues 90–107, 144–153, and 215–226), the lag times were set to 3, 4, and 3 ns, respectively.

Before the construction of the Markov state model, the trajectories were discretized using an algorithm of k-means clustering. The number of clusters, equal to thirty for the three regions of the polypeptide chain under consideration, was chosen by the heuristic method, which was described in the documentation for the PyEmma software package based on the VAMP-2 Score [37]. This clustering was used to build the Markov state model. Thus, the number of transitions from one state to another was calculated, the transition matrix was derived, and its eigenvalues and eigenvectors were calculated. The projections of cluster centroids, which were obtained in the discretization stage, onto the eigenvectors with the largest eigenvalues define the positions of the major states.

RESULTS AND DISCUSSION

Crystals of VchUPh and Relevant X-Ray Diffraction Data

High-quality crystals of uridine phosphorylase from the pathogenic bacterium *Vibrio cholerae* were grown in microgravity on board of the ISS. The three-dimensional structure of *Vch*UPh was determined at a record-high resolution of 1.04 Å.

Three-Dimensional Organization of the VchUPh Structure

The structural organization of the enzyme *Vch*UPh is similar to that of the *Vch*UPh structures reported previously [6, 8–10]. Each subunit of the *Vch*UPh molecule, which exists as a toroidal homohexamer with a diameter of ~106 Å, is composed of 253 residues (the molecular weight is 27.5 kDa). The secondary-structure elements of the monomer assigned with the DSSP program [38] include eight β-strands (28% of residues) and eight α-helices (32% of residue). The interdomain interface of each homodimer of the hexamer contains a Na^+ ion coordinated by three pairs of alike residues from adjacent subunits of the homodimer. Each dimer has two identical active sites formed by residues of adjacent subunits of the homodimer.

Active Site of VchUPh

The active sites of the enzyme molecule do not contain specific ligands but most of the ribose-binding subsites of the nucleoside-binding sites, which are formed by the residues Glu197 and Thr93 of one subunit and the residue His7 of the adjacent subunit of the homodimer [10], are occupied by the nonspecifically bound ethanediol and glycerol molecules. This fact can be attributed to the similar chemical nature of polyhydric alcohols and monosaccharide residues, which are aldehyde or keto alcohols. Almost in all active sites, glycerol molecules are hydrogen-bonded only to one residue of the ribose-binding site (Glu197 or His7).

In the structure of unligated *Vch*UPh determined previously at 1.22 Å resolution (PDB ID: 6EYP), almost all active sites contain glycerol in two conformations. One conformer is hydrogen-bonded only to the carboxyl group of Glu197, whereas another conformer is hydrogen-bonded to both residues (Glu197, His7).

In this structure, alcohol molecules bound to the ribose-binding subsite of the active site adopt one conformation but some of them are bound at partial occupancy. In the active site of the subunit D, the glycerol molecule is linked to the imidazole moiety of His7 of the adjacent subunit (NE2_His7/C–3.0 Å–O1_GOL) and the carboxyl group of Glu197 (OE2_Glu197/D–2.7 Å–O3_GOL, OE1_Glu197/D–3.3 Å–O3_GOL) (Fig. 2).

If the glycerol molecule is linked to both His7 and Glu197, its conformation and arrangement in the binding site of UPh are similar to the conformation of the C3'–O3'–C4'–O4'–C5'–O5' moiety of the ribose component of the substrates, pseudosubstrates, or inhibitors of UPh (uridine, thymidine, cytidine, and 2,2-anhydrouridine). However, there is a significant difference. Thus, in all the active sites of the structure under consideration, like in 6EYP, Thr93 that forms the flexible wall of the active site [6, 10, 11] is not hydrogen-bonded to the alcohol molecule and its side chain is at a distance of longer than 4–5 Å from the ligands. Unlike glycerol, the substrates and inhibitors are linked to the side chain of Thr93 through the O4'-hydroxy group, the position of which corresponds to the O2-hydroxy group of glycerol.

The glycerol binding in the active site was additionally investigated by molecular dynamics. In CD homodimer the residues 91–106 are located on the active-site wall of the subunit D. It is these residues that form the most clearly different alternative conformations. In both cases, the ligand occurs in the bound state only over a short period of time during the MD trajectory (~4.2 and 1 ns for the A and B conformations, respectively) (Fig. 3).

In the A conformation, in which the fragment 91–106 is located closer to the ligand (Fig. 2a), the binding to the active site was relatively stable for ~4.2 ns (Fig. 3a), and the average estimated binding free energy $\langle \Delta G_{LIE} \rangle = -14.4$ kJ/mol. However, during the first picoseconds, the conformation of the ligand drastically changed compared to the experimentally determined conformation, and the minimum estimated binding free energy ($\Delta G_{LIE}^{min} = -38.8$ kJ/mol) corresponded to this new conformation of glycerol in the binding site (Fig. 2b). In this conformation, the ligand is not hydrogen-bonded to the side-chain atoms of

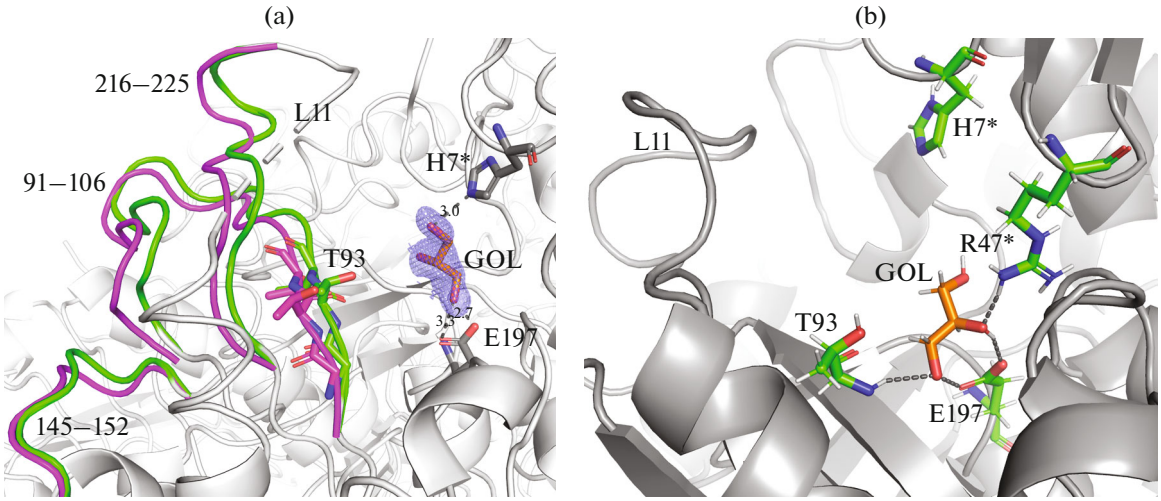

Fig. 2. (a) Three-dimensional organization of the enzyme active site in D(C) of *Vch*UPh (PDB ID: 6Z9Z). A fragment of the $2F_o–F_c$ electron density map is shown. Polar contacts between hydrogen-bond donors and acceptors are indicated by dashed lines. Residues of the carbon backbone and alternative conformations of the main chain are shown in different colors; residues of the C subunit are marked with an asterisk; L11 is the gate loop. (b) The structure of the enzyme active site (subunit D, A conformation) characterized by the minimum value of ΔG_{LIE} of the relative binding affinity of glycerol to *Vch*UPh.

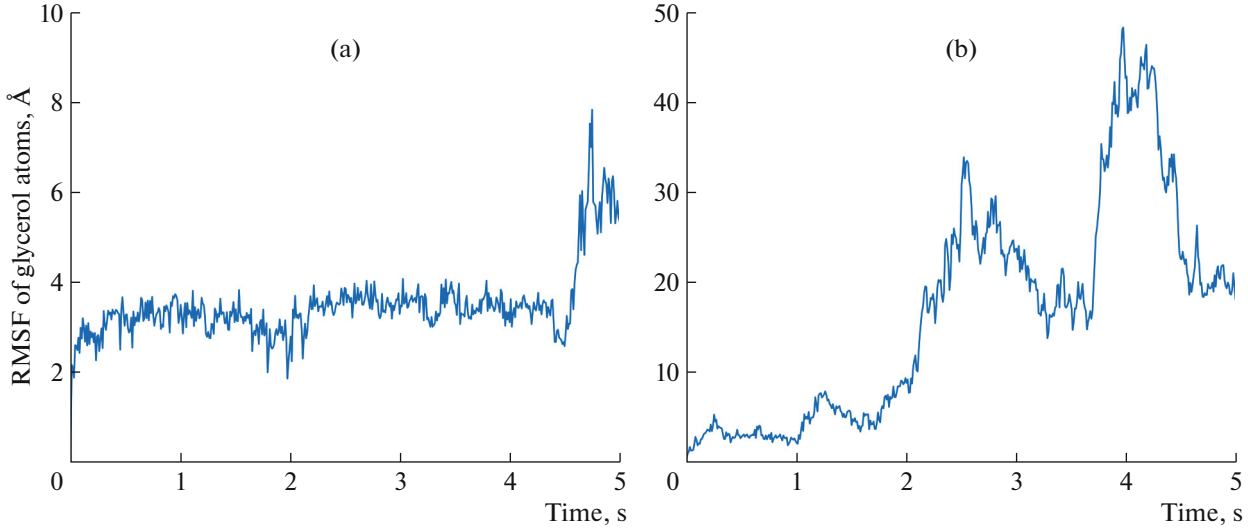

Fig. 3. Root-mean-square fluctuations (RMSF) of non-hydrogen atoms of glycerol during 6-ns MD simulations calculated for (a) the A conformation of fragments of the *Vch*UPh structure and (b) for the B conformation.

His7/C, but is linked to the main-chain amino group of Thr93/D and the side-chain atoms of Arg47/C. The residue Arg47 is involved in the phosphate-binding subsite of the active site, and Thr93 is involved in the β5-strand that forms the active-site wall.

In the B conformation, the fragment 91–106 is at a larger distance from the ligand (Fig. 2a), the binding was stable for a much shorter period of time (~1 ns) (Fig. 3b), and the average estimated binding free energy is higher ($\langle\Delta G_{\mathrm{LIE}}\rangle = -7.9$ kJ/mol) compared to the A conformation. Over the whole period during which the glycerol molecule was present in the active site of the enzyme, it did not form stable hydrogen bonds with Thr93 but, like in the A conformation, it was linked to Arg47/C of the phosphate-binding site. Taking into account all the aforesaid, it can be concluded that the binding stability and affinity of glycerol depend on the position and conformation of the β5-strand that forms the active-site wall. However, in all cases the binding stability of glycerol to the enzyme is lower compared to its substrates and competitive inhibitors.

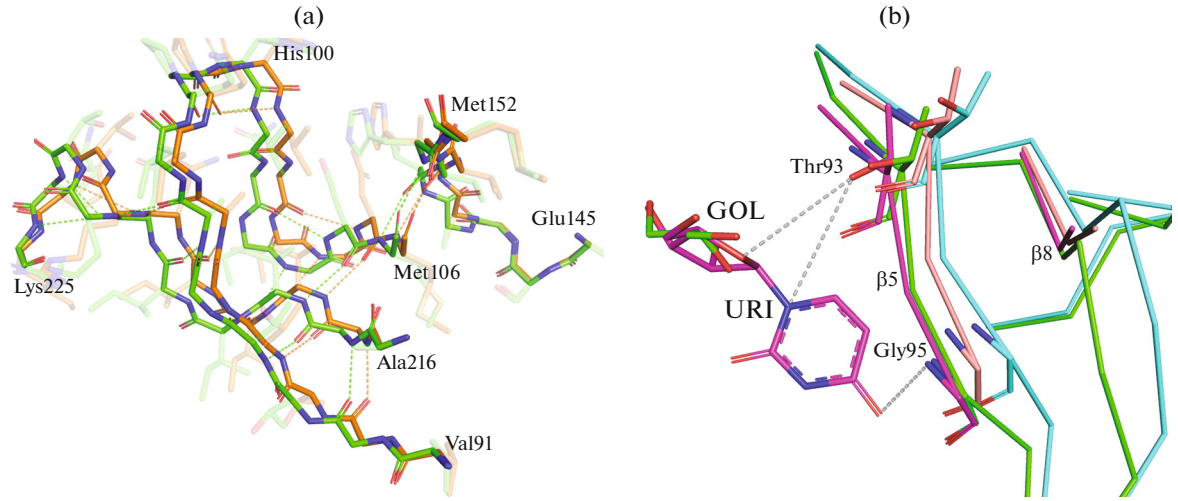

Fig. 4. Hydrogen-bond network between the main-chain atoms of fragments of the subunit D adopting alternative conformations in the three-dimensional structure of *Vch*UPh. (a) The alternative conformations are shown in different colors of the carbon backbone of the molecule. (b) The superposition of the three-dimensional structures of the β5- and β8-strands of *Vch*UPh in the ligand-free state (PDB ID: 6Z9Z) and in complex with uridine (PDB ID: 5M2T).

In all subunits, the position of the gate loop L11 [10] corresponds to the open state of the active site, like in the structure 6EYP, which is attributed to the fact that ethanediol and glycerol are not substrates of UPh, and the phosphate-binding site does not contain an orthophosphate anion.

Analysis of Alternative Conformations of Functionally Important Regions of VchUPh in the Ligand-Free State

In the subunits A, C, and F, the side chain of Arg47 involved in the phosphate-binding site adopts alternative conformations. The alternative conformations of this residue were observed earlier [6, 10, 11] in all structures, in which the phosphate-binding site does not contain coordinated orthophosphate or sulfate. As shown previously, the mobility of the side chain of arginine involved in the phosphate-binding site plays an important role in the binding of the orthophosphate anion and its arrangement with respect to the nucleoside molecule [10].

Alternative conformations of the spatially proximal regions 91–106, 145–152, and 216–225 of the subunit D are of great interest. Not only the side chains of these residues but also the main chains of these fragments have alternative conformations (Fig. 2).

In the high-resolution structures of *Vch*UPh in complexes with substrates [10], 6-methyluracil as the pseudosubstrate [6], and the inhibitor 2,2'-anhydrouridine [11], two positions of the β5- and β8-strand fragments were also observed upon the binding of the enzyme to the ligand at partial occupancy. One of these positions of the fragments of the tertiary-structure elements correspond to the ligated state, whereas another position corresponds to the ligand-free state. However, much shorter regions adopt two conformations (residues 92–95 and 217–219 in the structure of *Vch*UPh in complex with 2,2'-anhydrouridine [11]). Second, two positions were observed in the presence of the ligand at partial occupancy. Third, the residues in one of the two positions of the β5-strand fragment were linked to the ligand either directly (uridine, thymidine, 2,2'-anhydrouridine) or through a water molecule (6-methyluracil). In the subunit D of the structure described in this study, the glycerol molecule is present in the active site at full occupancy and it does no form significant bonds with the residues 92–94.

The fragments of the subunit D adopting alternative conformations include the following secondary-structure elements: the region 91–96 of the β5-strand, disordered regions with reverse turns 97–106 and 145–149, the starting fragment 150–152 of the β7-strand, the terminal fragment 216–221 of the β8-strand, and the starting fragment of the gate loop L11 (221–225).

The main-chain atoms of these fragments interact with each other through a hydrogen-bond network (Fig. 4a), and their movements in the molecule are apparently concerted. A scheme of conformational changes in the enzyme induced by the specific ligand, resulting in the closure of the active site, was proposed in [10]. The changes occur due to the concerted shift of the β5-strand, the β8-strand, and the gate loop L11 connected to the latter strand. However, the movement of the β5- and β8-strands in the structure under consideration occurs apparently independently of the binding of the specific ligand in the ribose-binding site. The transition of the active site to the fully closed conformation does not occur because, first, there is no interaction of the phosphate anion with the phos-

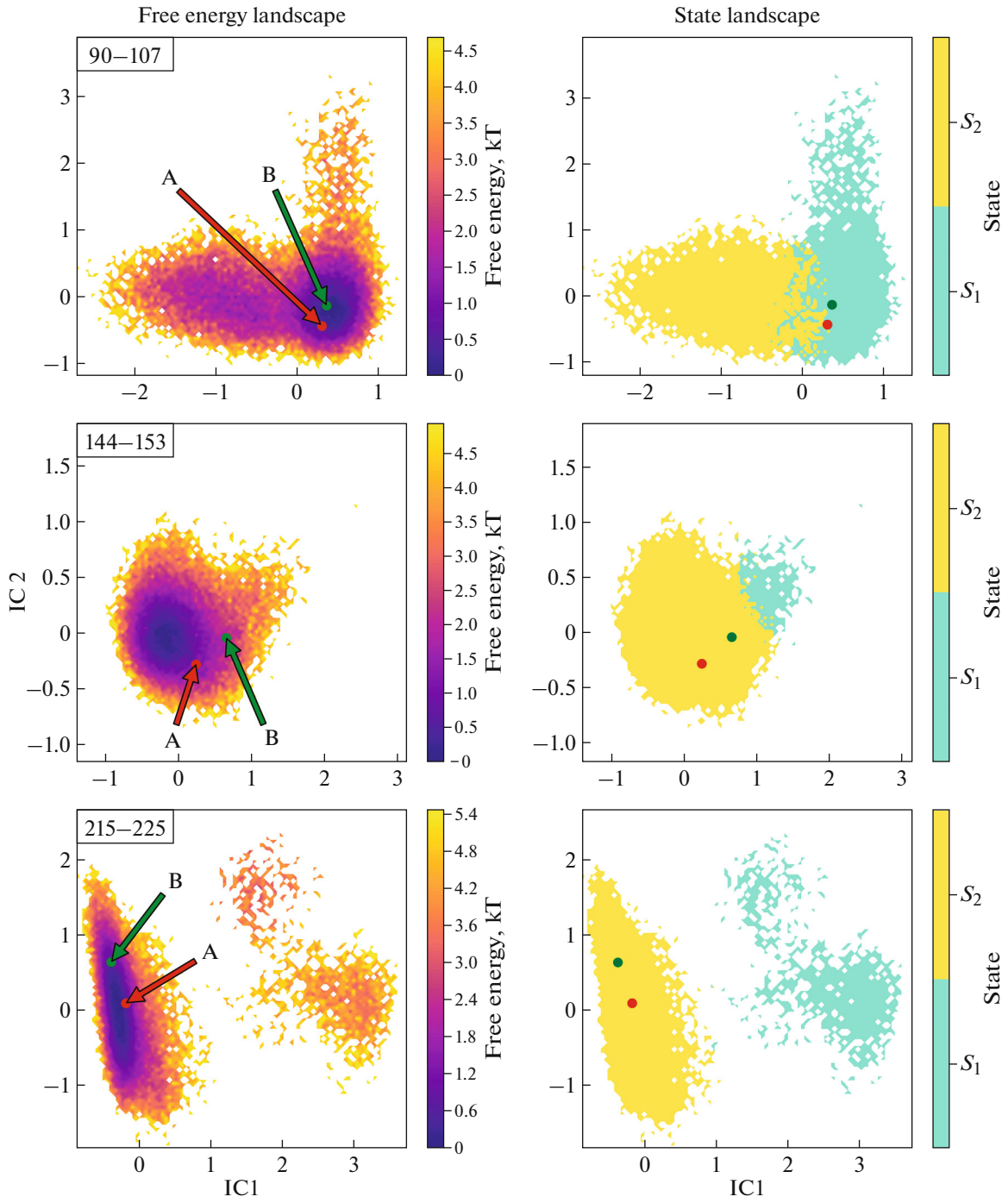

Fig. 5. Free energy landscapes for conformations of three fragments of the three-dimensional structure of *Vch*UPh calculated using Markov state models as a function of the two slowest independent components (IC) (left column). The landscapes for the longest-lived metastable states (right column). The conformations (A and B) of the fragments determined by X-ray diffraction are indicated by arrows.

phate-binding site and, second, the stabilization of the closed conformation apparently requires a strong interaction between the nucleoside or its analog and the residues 93–95 of the β5-strand (between the ribose moiety and Thr93 and between the pyrimidine moiety and the main-chain atoms of Gly95).

The less probable hypothesis is that the glycerol molecule, being bound in the ribose-binding site, induces conformational changes in the structure under study. However, there are no significant interactions, either direct of through a water molecule, between the glycerol molecule and the residues 93–95

of the β5-strand. Besides, even when the glycerol molecule is linked only to one residue of the nucleoside-binding site (subunit A), the β5-strand fragment also adopts alternative conformations analogous to those observed in the subunit D.

A comparison of the alternative conformations in the atomic-resolution structures of *Vch*UPh in the ligand-free state and in complex with uridine (PDB ID: 5M2T, 1.03 Å) shows that the alternative conformations of the β5- and β8-strands are similar to those observed in the structure under consideration (Fig. 4b). However, the atoms of the β5-strand in the conformation corresponding to the closed active site in the structure 5M2T, particularly of the region 93–94, are located closer to the ligand and the opposite wall of the active site (Fig. 4b). This confirms the hypothesis that the concerted conformational changes in the β5- and β8-strands can occur without the specific binding of the substrate or competitive inhibitors in the active site, but the transition to the fully closed state and stabilization of the latter are possible only upon the binding of the residues of the β5-strand to the specific ligands of the enzyme. Uridine, in turn, forms hydrogen bonds only with the residues 93–95 of the β5-strand in one (more closed) conformation.

In order to confirm or reject the hypothesis about the spontaneous transition between the conformations of the structural fragments under consideration, which does not depend on the ligand binding, we performed the conformational analysis with Markov state models. Figure 5 (left column) presents free energy landscapes for conformational clusters of the structural fragments depending on the values of the first two (slowest) independent components. Both experimentally determined conformations correspond to the approximately minimal value of the free energy and are within one potential well with no potential barriers between them. An analysis of the main stationary longest-lived states of the Markov model demonstrates that the experimental conformations belong to one stationary state (Fig. 5, right column); however, the points for the region 90–107 are close to the boundary of another Markov state. These data suggest that there is a rather free transition between the experimentally determined conformations of the fragments of the enzyme structure (residues 91–106, 145–152, and 216–225), which is not induced by the ligand binding but occurs spontaneously.

CONCLUSIONS

High-quality crystals of uridine phosphorylase from the pathogenic bacterium *Vibrio cholerae* were grown by the capillary counter-diffusion method in microgravity on board of the ISS. The three-dimensional structure of this enzyme was determined at atomic (1.04 Å) resolution. This is a record-high resolution for this enzyme. Alternative conformations of long fragments (β5-, β7-, and β8-strands and adjacent loops) of the protein molecules were found for the first time in the three-dimensional structure of uridine phosphorylase in the absence of specific bound ligands. Based on the X-ray diffraction data and conformational analysis by molecular dynamics and Markov state modeling, it was demonstrated that the concerted conformational changes of the β5-, β7-, and β8-strands can occur in the absence of the specific binding of the active-site residues to substrates, pseudosubstrates, or competitive inhibitors. The transition of the active site to the fully closed state and its stabilization are possible only upon the binding of the specific ligands to the residues of the β5-strand.

Glycerol molecules can bind in the ribose-binding subsite of the active site in a conformation similar to the conformations of moieties of natural substrates and inhibitors of the enzyme. However, the affinity and stability of this binding are low compared to the substrates and competitive inhibitors and depend, in particular, on the conformation and position of the β5-strand of the enzyme.

FUNDING

This study was performed within the framework of the Federal Space Program for 2016–2025 (the International Space Station Research and Development Program "Nauka"; crystallization by the counter-diffusion method and the X-ray diffraction data collection) and was financially supported by the Russian Foundation for Basic Research (project no. 19-29-12054; screening of crystallization conditions) and the Ministry of Science and Higher Education of the Russian Federation within the framework of the state assignment for the Federal Scientific Research Centre "Crystallography and Photonics" of the Russian Academy of Sciences (structure solution and refinement, analysis of the three-dimensional structure, including by molecular dynamics and Markov state modeling). The study was performed using facilities of the Center of Collective Use "Informatics" of the Federal Research Center "Informatics and Management" of the Russian Academy of Sciences [39].

CONFLICT OF INTEREST

The authors declare no conflict of interest, financial or otherwise.

REFERENCES

1. K. Katsumata, H. Tomioka, T. Sumi, et al., Cancer Chemother. Pharmacol. **51** (2), 155 (2003). https://doi.org/10.1007/s00280-003-0583-2
2. A. Kanzaki, Y. Takebayashi, H. Bando, et al., Int. J. Cancer **97** (5), 631 (2002). https://doi.org/10.1002/ijc.10105
3. C. Luccioni, J. Beaumatin, V. Bardot, et al., Int. J. Cancer **58** (4), 517 (1994). https://doi.org/10.1002/ijc.2910580411
4. A. A. Lashkov, N. E. Zhukhlistova, S. E. Sotnichenko, et al., Crystallogr. Rep. **55**, 41 (2010).
5. T. T. Caradoc-Davies, S. M. Cutfield, I. L. Lamont, et al., J. Mol. Biol. **337**, 337 (2004). https://doi.org/10.1016/j.jmb.2004.01.039
6. I. I. Prokof'ev, A. A. Lashkov, A. G. Gabdulkhakov, et al., Crystallogr. Rep. **63**, 418 (2018).
7. A. A. Lashkov, N. E. Zhukhlistova, A. G. Gabdoulkhakov, et al., Acta Crystallogr. D **66**, 51 (2010). https://doi.org/10.1107/S0907444909044175
8. A. A. Lashkov, A. G. Gabdulkhakov, I. I. Prokofev, et al., Acta Crystallogr. F **68**, 1394 (2012). https://doi.org/10.1107/S1744309112041401
9. I. I. Prokofev, A. A. Lashkov, A. G. Gabdulkhakov, et al., Acta Cryst. F. **70**, 60 (2014). https://doi.org/10.1107/S2053230X13031877
10. I. I. Prokof'ev, A. G. Gabdulkhakov, V. V. Balaev, et al., Crystallogr. Rep. **61**, 964 (2016).
11. P. A. Eistrikh-Heller, S. V. Rubinskii, I. I. Prokof'ev, et al., Crystallogr. Rep. **65**, 269 (2020).
12. A. M. Daa Silva Neto, J. R. Torini de Souza, L. Romanello, et al., Biochimie **125**, 12 (2016). https://doi.org/10.1016/j.biochi.2016.02.007
13. T. P. Roosild, S. Castronovo, A. Villoso, et al., J. Struct. Biol. **176**, 229 (2011). https://doi.org/10.1016/j.jsb.2011.08.002
14. I. P. Kuranova and M. V. Koval'chuk, Priroda, No. 3, 12 (2014).
15. E. H. Snell and J. R. Helliwell, Rep. Prog. Phys. **68** (4), 799 (2005). https://doi.org/10.1088/0034-4885/68/4/r02
16. K. M. Boiko, V. I. Timofeev, V. R. Samygina, et al., Crystallogr. Rep. **61**, 718 (2016).
17. Yu. A. Abramchik, V. I. Timofeev, T. I. Murav'eva, et al., Crystallogr. Rep. **61** (6), 974 (2016).
18. W. Kabsch, Acta Crystallogr. D **66**, 125 (2010). https://doi.org/10.1107/S0907444909047337
19. P. Evans, Acta Crystallogr. D **62** (1), 72 (2006). https://doi.org/10.1107/S0907444905036693
20. A. Vagin and A. Teplyakov, J. Appl. Crystallogr. **30** (6), 1022 (1997). https://doi.org/10.1107/S0021889897006766
21. P. V. Afonine, R. W. Grosse-Kunstleve, N. Echols, et al., Acta Crystallogr. D **68**, 352 (2012). https://doi.org/10.1107/S0907444912001308
22. P. Emsley, B. Lohkamp, W. G. Scott, et al., Acta Crystallogr. D **66**, 486 (2010). https://doi.org/10.1107/S0907444910007493
23. R. A. Laskowski, M. W. MacArthur, D. S. Moss, et al., J. Appl. Crystallogr. **26** (2), 283 (1993). https://doi.org/10.1107/S0021889892009944
24. I. W. Davis, A. Leaver-Fay, V. B. Chen, et al., Nucl. Acids Res. **35**, 375 (2007). https://doi.org/10.1093/nar/gkm216
25. D. Van Der Spoel, E. Lindahl, B. Hess, et al., J. Comput. Chem. **26**, 1701 (2005). https://doi.org/10.1002/jcc.20291
26. A. D. MacKerell, Abstracts Papers Am. Chem. Soc. **216**, 696 (1998).
27. J. Huang, S. Rauscher, G. Nawrocki, et al., Nat. Methods **14**, 71 (2016). https://doi.org/10.1038/nmeth.4067
28. K. Vanommeslaeghe, E. Hatcher, C. Acharya, et al., J. Comput. Chem. **31**, 671 (2010). https://doi.org/10.1002/jcc.21367
29. M. Parrinello and A. Rahman, J. Appl. Phys. **52**, 7182 (1981). https://doi.org/10.1063/1.328693
30. G. Bussi and M. Parrinello, Comput. Phys. Commun. **179**, 26 (2008). https://doi.org/10.1063/1.3073889
31. J. Aqvist and J. Marelius, Comb. Chem. High Throughput Screen **4** (8), 613 (2001). https://doi.org/10.2174/1386207013330661
32. C. Schutte, A. Fischer, W. Huisinga, and P. Deuflhard, J. Comput. Phys. **151**, 146 (1999). https://doi.org/10.1016/S1570-8659(03)10013-0
33. C. Wehmeyer, M. K. Scherer, T. Hempel, et al., Living J. Comp. Mol. Sci. **1**, 5965 (2019). https://doi.org/10.33011/livecoms.1.1.5965
34. G. Perez-Hernandez, F. Paul, T. Giorgino, et al., J. Chem. Phys. **139**, 015102 (2013). https://doi.org/10.1063/1.4811489
35. B. E. Husic and V. S. Pande, J. Chem. Phys. **147**, 176101 (2017). https://doi.org/10.1063/1.5002086
36. B. Trendelkamp-Schroer, H. Wu, F. Paul, and F. Noé, J. Chem. Phys. **143**, 174101 (2015). https://doi.org/10.1063/1.4934536
37. R. T. McGibbon and V. S. Pande, J. Chem. Phys. **142**, 124105 (2015). https://doi.org/10.1063/1.4916292
38. W. Kabsch and C. Sander, Biopolymers **22**, 2577 (1983). https://doi.org/10.1002/bip.360221211
39. Regulations on the Collective-Use Center "Informatika." http://www.frccsc.ru/ckp

Translated by T. Safonova